Overview of Australian R&D in Mine Imaging

R.J.Wyber
Midspar Systems Pty Ltd
24 Farrer Place
Oyster Bay NSW 2225 Australia
rjwyber@ozemail.com.au

I. INTRODUCTION

The Australian program in mine imaging was carried out under the Capability and Technology Demonstrator Program. The work on mine imaging was carried out by Midspar Systems in collaboration with DSTO. The aim of the program was to integrate advances in wide band technology to develop a system capable of detecting, localizing and classifying all mine types including stealth mines both on the sea floor and buried. The program ran from 1999 until 2006.

A fundamental part of a project such as this is to understand the nature of the acoustic signals reflected from various mine types and an extensive program was conducted to measure these over a wide frequency band. From the measured data it proved possible to model the impulse response returned from the mine quite accurately using very simple models. Using the impulse response measured in a controlled environment, various imaging algorithms were evaluated and adapted to the unique characteristic of the sonar signal.

The final stage of the program was to develop a system capable of carrying out the sonar measurements and overcome the complexities of an operational environment on the floor of Sydney Harbour.

II. MEASUREMENT OF THE IMPULSE RESPONSE OF THE TARGETS

A. Characteristics of the Test Signals

Three different sonars were used for the measurements covering the bands 1 to 10 kHz, 22 to 66 kHz and 100 to 200 kHz. The wide bandwidths of these sonars allow the band limited impulse response of the targets to be measured over the different frequency ranges. To obtain a high signal to noise ratio it is desirable to transmit a long broadband test signal. This may be compressed to a band limited impulse by multiplying the frequency spectrum by a matched filter which has the conjugate phase of the transmitted signal and an amplitude which combines with the system response to give the desired window for the band limited impulse. For the measurements a Kaiser-Bessel window was used which allowed the trade-off between leakage of the impulse outside the main lobe and the width of the impulse to be optimized for the target.

While a Linear Frequency Modulated pulse (LFM) is commonly used for sonar measurements, a Linear Period Modulated pulse (LPM) has the highly desirable property that it is Doppler tolerant. This means that the full processing gain is achieved and the impulse response is formed even in the presence of a Doppler shift in the received signal [1]. The only effect of Doppler is to generate a time displacement in the impulse position which must be corrected prior to combining multiple impulses to form an image, where it is significant. For this reason the LPM pulse was used for most of the measurements.

An alternate test signal which was evaluated was a sequence of Gold codes [2]. While these have significant leakage outside the main lobe of the impulse and are not Doppler tolerant they have the property that pulse compression may be achieved on the coded sequence using aperiodic correlation. Also multiple Gold codes of the same length exist which are not correlated with each other. This property allows multiple pulses to be transmitted without waiting for the reverberation from the previous pulse to decay. This is a useful property for synthetic aperture sonar where typically the speed of advance is limited by the need for the previous pulse to decay before the sonar reaches the position of the next virtual sensor. It also allows the time required to acquire sufficient impulses for tomographic imaging to be reduced by an order of magnitude.

B. Characteristics of the Target Impulse Response

When the wavelength is much smaller than the dimension of the target the target impulse can be well represented as the sum of the rigid body reflection, in which the reflections are caused by specular facets and discontinuities on the body, and the structural response. The structural response is caused by mechanical waves being excited in the target and then re-radiating as they propagate.

For targets with a thick case such as the Mk 84 bomb the impulse response is dominated by the rigid component, although there is evidence of structural waves near broadside and end-fire. A very simple model [3] allows the impulse response to be estimated as

$$I(t)=\kappa\partial^2A(t)/\partial t^2 \qquad (1)$$

978-1-4244-5222-4/10/$26.00 ©2010 IEEE

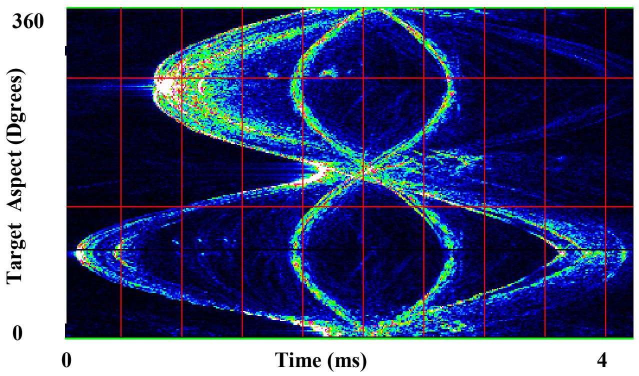

Fig. 1 The impulse response from the Mk84 bomb as it is rotated through 360 degrees in the band 100 to 200 kHz.

where A(t) is the cross-section area of the target insonified at time and
κ is a constant.

C. MK84 Bomb at High Frequencies

From eq. 1 the Mk84 bomb generates impulses from the corners at the rear of the bomb, the nose and the lifting eyes at all aspects and specular reflections from the end, the nose and the side for a limited range of aspect angles. As the target rotates about a horizontal axis the arrival times of these impulses varies sinusoidally relative to the point of rotation. These features fully define the target response given in fig. 1. In this figure the center pair of sine waves are from the lifting eyes, the sine wave near the bottom left is from the nose and the pair at the upper left are from the tail.

D. Thin Wall Cylinder at High Frequencies

For a thin walled cylinder at the same frequencies the response differs dramatically as shown in fig. 2. The rigid component from the ends of the cylinder trace a sinusoidal path as the target rotates. There is however a very strong additional component due to the structural waves in the target. For defined shapes such as spheres or cylinders it is possible to derive an analytic expression for the impulse response. An alternative method with more general application is to:

1. model the structural waves which may propagate in the target,
2. identify points where the flexural waves can radiate energy back to the target, which occurs when the component of the group velocity in the direction of the target matches the speed of sound in water and
3. determine the coupling of the incident signal into the flexural wave.

Solving the equations for the flexural waves provide five possible waves. Two of these are highly attenuated and do not propagate and two are coincident over the frequencies of interest. This leaves two distinct propagating flexural waves.

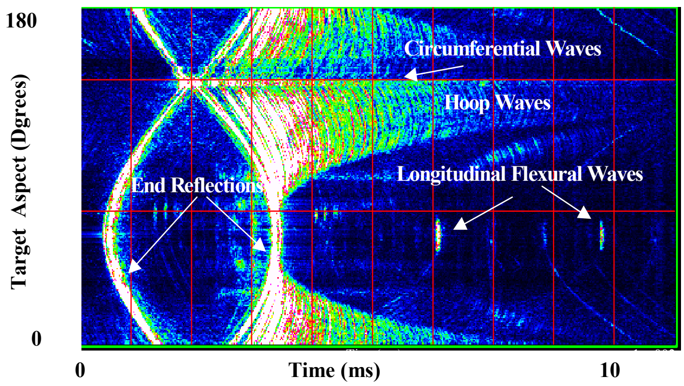

Fig. 2 The impulse response for the air filled cylinder as a function of the target aspect.

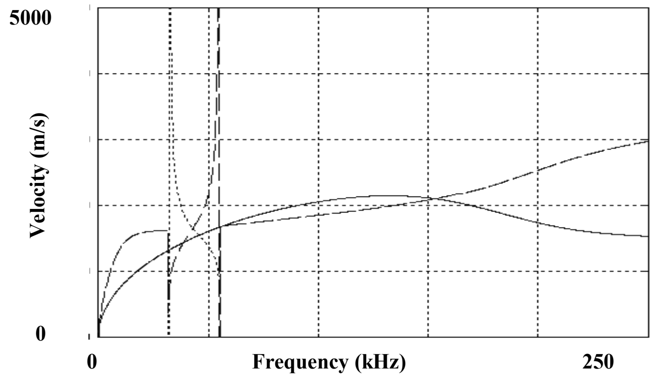

Fig. 3 The group velocity of the waves propagating in the shell of the cylinder.

While both of these propagate in both the plate and fluid at the boundary, one is predominantly in the fluid and the velocity tends asymptotically to the velocity of sound in water at high frequencies. The other pair are predominately in the shell and the velocity tends asymptotically to that of the shear wave at high frequencies. As the velocity of the flexural wave varies with frequency and is therefore dispersive, it is the group velocity which determines the speed of propagation. This is plotted in fig. 3 and it may be seen that in the region 100 to 200 kHz both waves exceed the speed of sound and have the potential to radiate energy.

To validate the model a time frequency analysis was carried out on the signal reflected from the cylinder at broadside. This analysis was carried out by developing a modified form of the Gabor Spectrogram [4] which used a Kaiser-Bessel gating function. This allowed better rejection of the leakage from the strong specular return. When this was done the response of fig. 4 was measured. By separating the impulse response received at the target in frequency it was possible to identify two pulse trains associated with the propagation of the flexural waves around the cylinder. The upper pulse train is more highly attenuated and decays after circling the cylinder three times. This is associated with the wave in the shell and shows

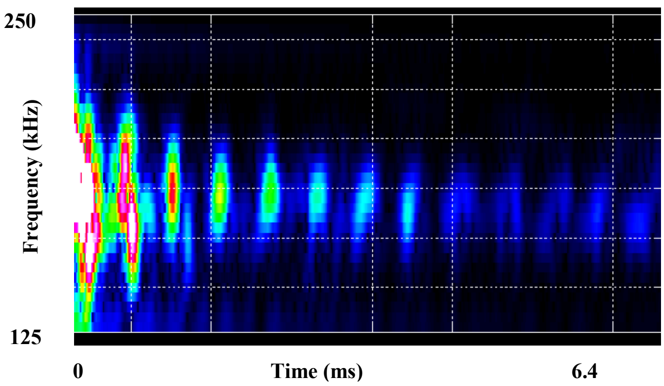

Fig. 4 The measured time frequency response from the flexural waves circling the cylinder at broadside.

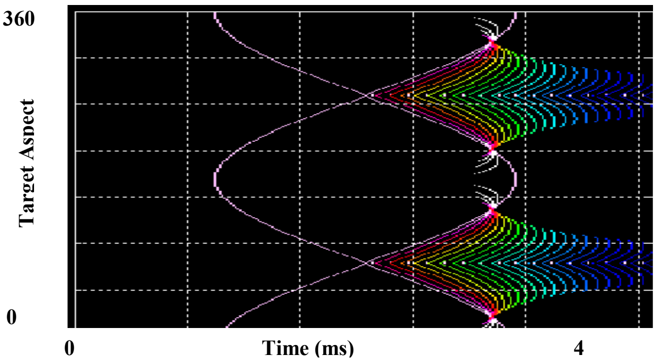

Fig. 5 The reflections from the ends of the cylinder and the hoop waves predicted by the model.

a slight decrease in the arrival time as the frequency increases. This is the wave with the group velocity which continues to increase with frequency. The other wave is the wave in the water which has a lower attenuation and is still evident after circling the cylinder thirteen times. The delay of these impulses increases slightly with frequency as the group velocity decreases.

For other target aspects the wave directly coupled into the walls of the cylinder tends to propagate away from the target and does not radiate in the target direction. There are however, a family of similar waves designated as hoop waves which are excited from the incident pressure on the back of the cylinder and propagate back towards the target while circulating around the cylinder. The response modeled for these waves is plotted in fig. 5. The modeled response may be seen to accurately predict the measured result.

E. The Mk82 Bomb at Low Frequencies

At frequencies between 1 kHz and 10 kHz the response from the bombs with a thick shell differs significantly from the high frequency response. In fig. 6 the response of the Mk82 bomb without fins is plotted as the target aspect is varied over 360 degrees. While the rigid body response associated with the nose and the tail remains evident the latter part of the response is dominated by structural waves.

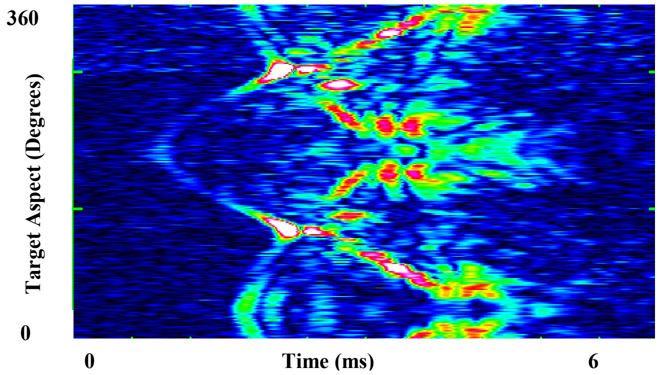

Fig. 6 The impulse response of the Mk82 bomb as the target aspect varies for freauencies from 1 to 10 kHz.

III. THE IMAGES FORMED FROM DATA MEASURED IN THE TEST FACILITY

F. The Mk84 Bomb at High Frequencies

The Mk84 bombed rigged on the test facility is shown in fig. 7. The images formed of the bomb using both of the high frequency test bands are shown in fig. 8. The differences in the image at the tail of the bomb is due to the presence of a plate for one measurement but not the other and not due to the difference in the frequency bands. Apart from a slight loss of resolution in the lower band the images are similar. In forming these images the modulus of the analytic signal formed from the impulse response is used as an input to the imaging algorithm. While this decreases the resolution to some extent it eliminates the ringing in the impulse response which arises from the use of a band limited signal.

G. The Mk84 Bomb at Low Frequencies

In fig. 9 the image shown is formed from the MK84 bomb in the frequency band 1 to 10 kHz. The processing differs slightly from that used in the higher frequency band in that the impulse response is used rather than the analytic signal. This causes the ringing evident around the boundary of the image. It does however compensate to some extent for the loss of resolution in the low frequency band. The shape of the bomb is clearly discernible which demonstrates the potential to use these low frequencies, which penetrate the sediment, to image buried mines. In forming this image the impulse response was gated to reduce the contribution from the structural waves.

H. The Air Filled Cylinder

The image formed for the air filled cylinder is shown in fig. 10. While the thin cylinder may be seen in the center of the image the more spectacular parts are generated by the structural waves. While these demonstrate that the target is man made they do not greatly help in recognizing the target and more realistic images are formed by gating out the structural waves.

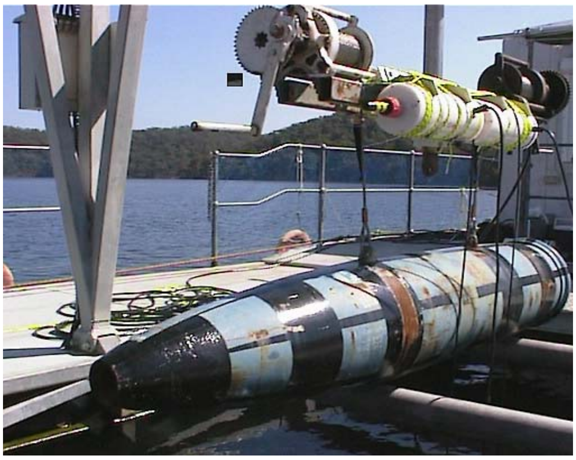

Fig. 7 The Mk 84 bomb rigged on the testfFacility.

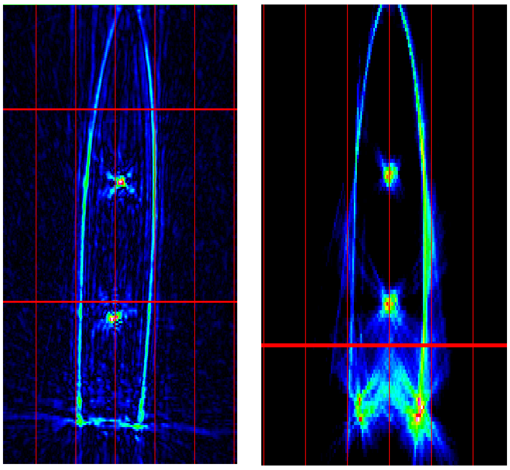

Fig 8 Tomographic image formed of the Mk84 bomb (100-200 kHz left), (22-66 kHz right).

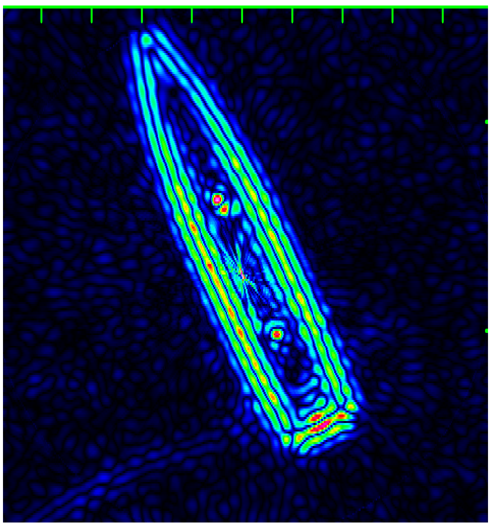

Fig. 9 The image of the Mk84 bomb formed using the band 1 to 10 kHz.

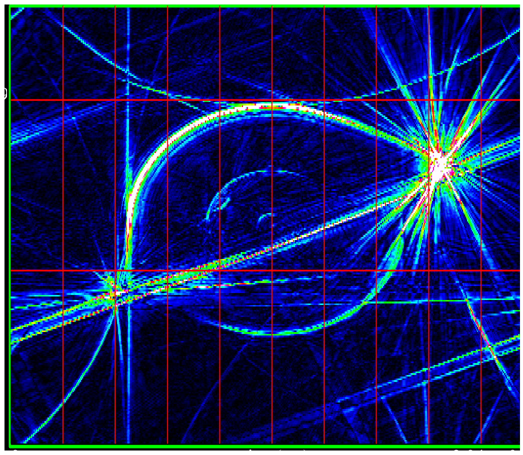

Fig. 10 The image formed from the air filled cylinder.

I. Imaging Using Gold Codes

The incentive to use Gold codes is to allow successive pulses to be transmitted before the signal from the previous pulse has fully decayed. The potential range ambiguities which can arise from this are avoided by using a sequence of different pulses which have a low correlation. The desirable property for a family of coded sequences used in this role, is that they correlate with themselves to give an ideal impulse response and are uncorrelated with each other. While M-sequences correlate to give an ideal impulse response, it is necessary to use a periodic correlation which does not eliminate the range ambiguity. Gold codes provide a reasonable approximation to the ideal code. The limitation with the Gold codes is that there is leakage from the perfect impulse at a level which is ($1/\sqrt{N}$) where N is the length of the sequence. This increases the contribution from the reverberation. The Gold codes used for the measurements were of length 1024 points which allowed them to be transmitted at a rate of eight per second.

The image formed using Gold codes in the test facility is shown in fig. 11. There is no degradation evident from the leakage of the impulse response even though the measurement was made in 12.5% of the time taken using the LPM pulse. Further measurements using the Gold codes were carried out in Sydney Harbour. For these measurements the processing load increased as it was necessary to correlate the received signal with multiple Doppler shifted replicas to obtain an impulse response. The reverberation level increased by 9 db because of the side lobe leakage. This additional reverberation is however uncorrelated between pulses and the full processing gain of the high resolution imaging is available to reduce its level. This is not always the case once the high resolution imaging resolves the structure of the reverberation.

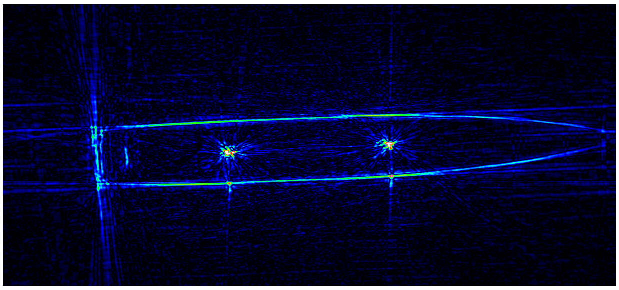

Fig. 11 The image formed of the Mk84 bomb using Gold codes.

IV. INTERFEROMETRY

J. The Height of the Point of Radiation on a Tilted Cylinder

Interferometry uses a pair of hydrophones displaced vertically to measure the phase of the reflected signal. As the signals reflected from the target are formed by the sum of impulse responses, in general only one impulse response is present in any range cell. The phase between the signal at the two hydrophones is then a measure of the height of the reflector on the target and a 3-dimensional image may be formed. An example of this is given in fig. 13 which shows the phase between two hydrophones separated vertically by 1 meter for the signal reflected from the air filled cylinder. The cylinder is tilted downwards at one end. The color green corresponds to transmission of the reflected wave from a low point on the cylinder and purple to a high point. In the upper half of the display the high end is furthest away from the hydrophones and flexural waves are radiated from a point on the cylinder which becomes lower as the flexural waves travel along the cylinder from the back. In the lower half of the display the high end is closest to the hydrophones. This display provides further validation of the m`odel for the cylinder.

K. Imaging of the Manta Practice Mine

Fig. 13 shows a photo of the Manta practice mine and the 2-Dimensional image formed in the test facility. The outer rim of the mine and the central plate are evident in this image. The four points forming a square inside the circle of the rim are from the lifting eyes and their mounting points. There is further structure at the top and bottom in the center of the image which are from internal ribs. All of these features are evident in the left image of fig. 14. This is a 3-D image formed using the interferometery and in this image the features are separated in height. In forming this image a threshold was set which eliminated the reflections from the outer shell. When this threshold is lowered the image on the right of fig. 14 is formed. This image shows the outer shell and two hydrophones hanging below the mine.

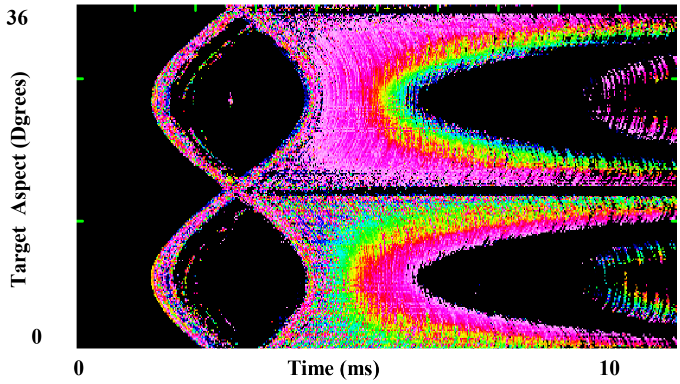

Fig. 13 The phase of the impulse response for the air filled cylinder as a function of the target aspect.

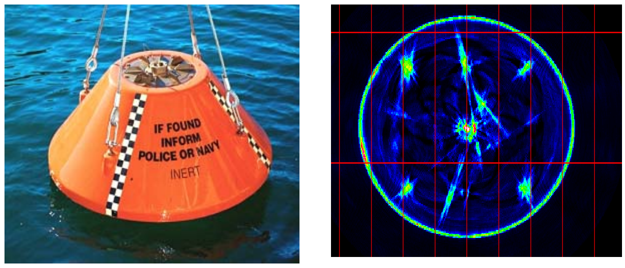

Fig. 13 The Manta practice mine together with its 2-Dimensional image.

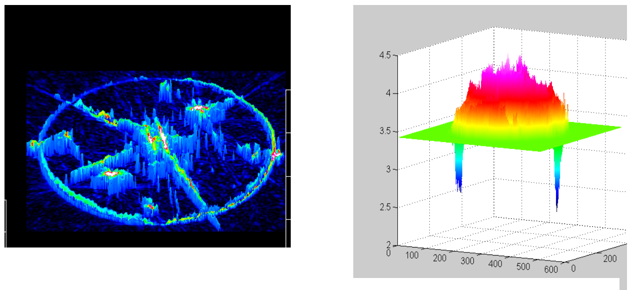

Fig. 14 The 3-Dimensional image of the Manta practice mine with two different threshold levels.

V. MEASUREMENTS IN AN OPERATIONAL ENVIRONMENT

L. Synthetic Aperture Sonar

To evaluate the imaging algorithms in an operational environment, measurements were carried out at HMAS Penguin in Sydney Harbour. This was a fairly harsh environment with a sand bottom, a significant swell coming through the heads and a strong velocity profile due to fresh water flowing from upstream. The initial synthetic aperture sonar measurements were made using the DERA rail and a sonar with 32 receive elements and a bandwidth from 118 to 182 kHz. There was significant movement of the rail with a period of about 10 seconds due to wave motion in addition to fluctuations in the speed of sound over the propagation paths.

Techniques evaluated to compensate for the time fluctuation included the displaced phase center algorithm (DPCA), measurement of the propagation time to hydrophones in the water column and measurement of the propagation time for signals reflected from target highlights. While all of these allowed images to be formed it was found that the target strength to reverberation after processing was in the order of 50 dB. While such high signal to reverberation is desirable it also meant that side lobes tended to smear the response and mask areas of the image. To avoid this a Kaiser-Bessel weighting window was applied to the synthetic element data to achieve side lobe suppression of 60 dB. It was found that to realize this level of suppression it was necessary, that in compensating for the fluctuations in the arrival time, the phase accuracy was better than 6 degrees. By effectively averaging the arrival times measured over all of the real elements in the receiving array for a signal reflected from a target highlight, it proved possible to achieve a timing error corresponding to a distance of about 80 microns. This satisfied the criteria.

The images from a Mk84 bomb and a Stonefish exercise mine, formed with this high side lobe suppression are shown in fig. 15. The lack of reverberation evident in the vicinity of the target is a consequence of the vertical beam width of the transmitter which is focused on the sea floor past the two targets. Due to the range of measured aspect angles being limited to about 20 degrees and the aspect of the targets the specular returns which define the outline of the case of the bomb were not received. The highlight associated with the corners and various features on the mines do however define the size and aspect of the targets. The reverberation is resolved to show the structure of the bottom rather than appearing as a random noise contribution.

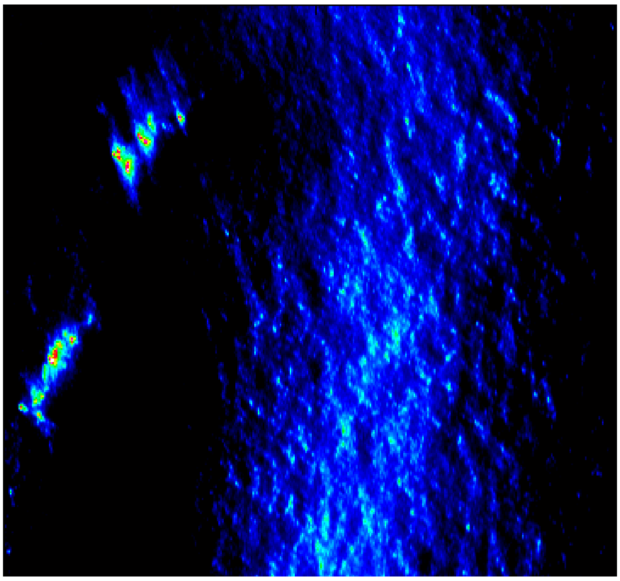

Fig. 15 The synthetic aperture image of the Mk84 bomb (top) and the Stonefish exercise mine.

M. Tomographic Imaging

The transducer for the parametric sonar weighed several hundred kilograms which would have required a substantial vessel if this was to be deployed over the side. This was in conflict with the requirement of a small highly maneuverable vessel which was required to accurately circumnavigate the targets. It was also necessary to be able to deploy the higher frequency sonars, one of which weighed about 90 kg. To solve this, a catamaran, the Littoral Surveyor, was custom built. It incorporated a tower and moon well in the aft deck, through which the transducers were deployed. The associated transmit, processing and receive equipment which weighed a further 1000 kg were all placed in shock mounted racks in the cabin. The test vessel is shown in fig. 16. The 150 kHz sonar configured for interferometry measurements is shown being prepared for deployment through the moon well in fig. 17.

The tomographic measurements were made by circumnavigating the targets at a range of 50 m. Because of the wide bandwidth of the sonars the reverberation is sufficiently reduced that the targets can be detected with a single pulse despite the wide beam width. The impulse response of the Manta practice mine is shown in fig. 19. This response is aligned using the reflection from the rim. The image formed of the practice mine is plotted in fig. 20.

Fig. 17 The custom built test vessel.

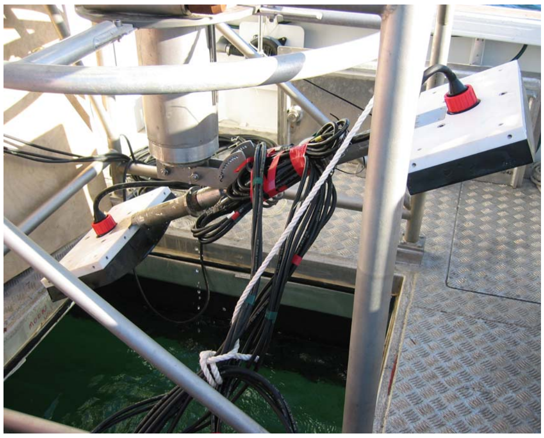

Fig. 18 The interferometeric sonar and the moon well.

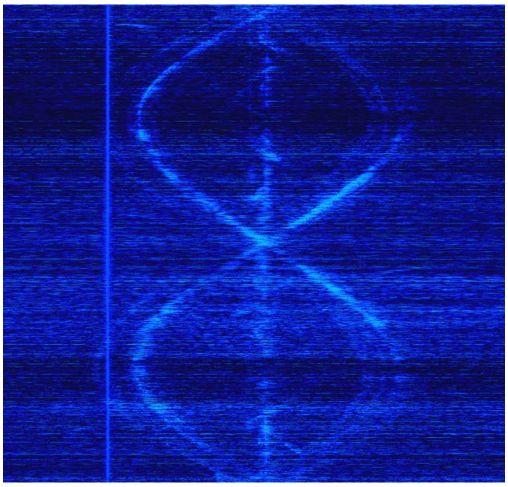

Fig. 19 The impulse response of the Manta practice mine on the sea floor.

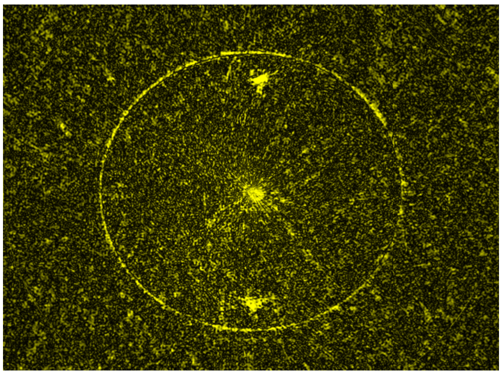

Fig. 20 The image of Manta practice mine on the sea floor.

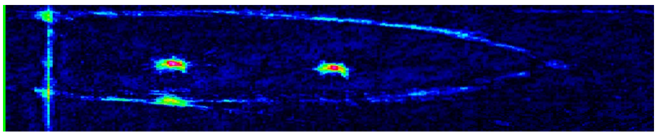

Fig. 21 The image of the Mk84 bomb on the sea floor.

In fig 21 the image of the Mk84 bomb on the sea floor is plotted. Due to the circumnavigation of the target which ensonifies all aspects of the target the complete outline of these targets is well defined. The plate in the center of the Manta mine is also visible. The remaining two points in both images are from fiberglass poles used to mount hydrophones on the targets. While neither of the alignment techniques used to form these images is suitable for an operational sonar, the alignment accuracy required to form these images is an order of magnitude less than that required to provide high side lobe suppression with a synthetic aperture sonar. It is anticipated that proven methods of aligning the data using the reverberation could be readily adapted for tomographic imaging. These were not investigated for these measurements as only a single sensor receiving array was available. It was however demonstrated that correlation of the images formed from two successive circles around the target allowed the drift in the position estimate which arises from an INS system to be measured and compensation applied. This avoids the need to use a GPS signal to maintain an INS system in alignment and allows an underwater vehicle to maintain accurate INS position data while submerged.

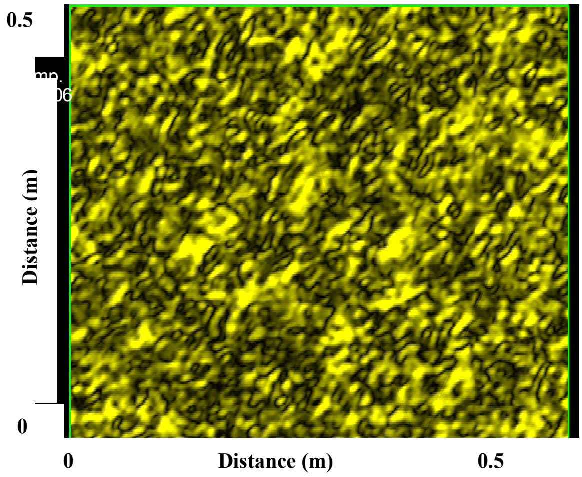

Fig. 22 The sea floor in the vicinity of the mines.

Fig. 22 shows the sea floor. With the resolution achieved, this is resolved into an image rather than being a random background noise as is commonly assumed in sonar calculations. Photographs of the sea floor show sea grass and holes from burrowing animals which contribute to the structure which is evident.

While the Manta practice mine is nominally a stealth mine the structure detected is from the rigid part of the mine at the rim, the center plate and the poles. This raises the issue as to how a stealth mine composed entirely from fiberglass could be detected. The solution to this was somewhat surprising and is an outstanding example of why experiments at sea are necessary. The Manta practice mine on the sea floor which is covered by sea grass is shown in fig. 23. Fig. 24 shows the 3-Dimensional image which is formed for the mine. This image is formed only from the phase difference of the reflected signal between the receiving hydrophones, and was expected to show the height of the dominant reflectors above the sea floor. Instead it appears that the image is the apparent height of the sea floor. In the interior of the mine the height of the sea floor is increased by about 20 cm near the rim and 10 cm near the center. This is attributed to a disturbance of the sound wave as it propagates through the fiberglass shell of the mine. Refraction does not explain the amount by which the sea floor is raised. Modeling the flexural waves in the shell did however predict a coupling mechanism which not only

Fig. 23 The Manta practice mine in the sea grass on the sea floor.

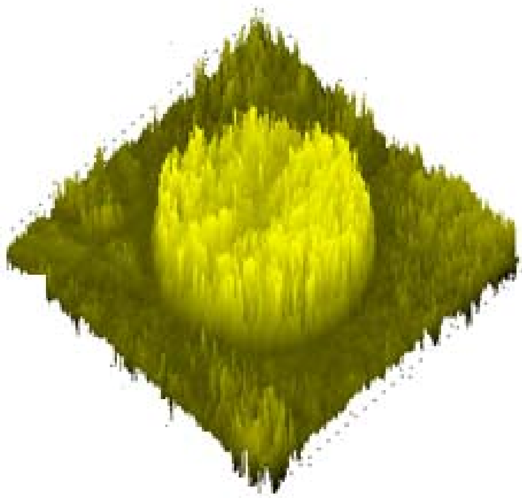

Fig. 24 The 3-Dimensional image of the Manta practice mine on the sea floor.

predicted the observed increase in the apparent height of the sea floor but also predicted the observed decrease in this height towards the center of the mine. This is potentially a mechanism which will allow true stealth mines to be detected and classified.

VI. DETECTION OF BURIED MINES

The principal role of the parametric sonar operating in the band 1 to 10 kHz was to detect buried mines. The sonar had a beam width of about 3 degrees which was much less than the yaw of the vessel about the nominal track as it circumnavigated the target. It was therefore necessary to integrate the navigation system of the vessel with the sonar to maintain the beam on the target as the vessel aspect varied.

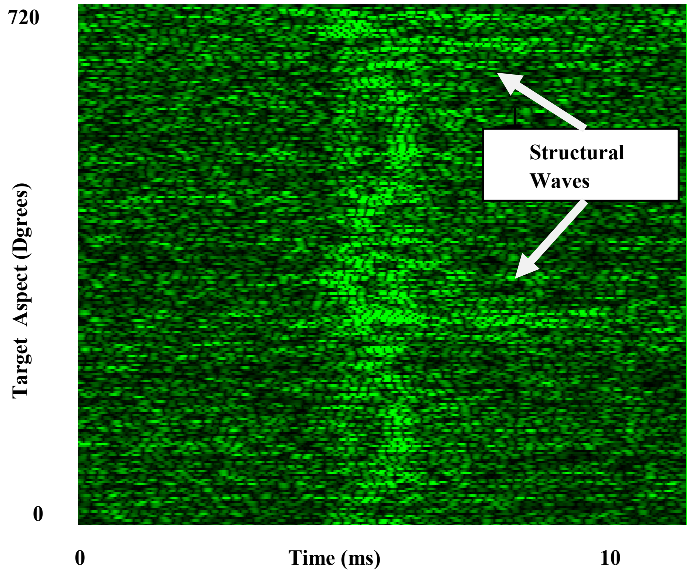

Fig. 25 The impulse response from the buried Mk82 bomb as the sonar circumnavigates the target.

The impulse response of the buried Mk82 bomb measured as the sonar circumnavigated the target twice is plotted in fig. 25. While there are two fiberglass poles proud of the surface on the mine there is much more structure in the impulse response than can be attributed to these alone. In particular the target structural waves match those observed in the test facility which are plotted in fig. 6. These allow the aspect of the mine to be identified from the impulse response alone.

When using a parametric sonar the phase of the low frequency secondary signal remains fairly constant over the width of the footprint of the sonar on the sea floor. Because of this there is strong correlation between successive pings provided there is overlap of the footprint between pings. This allows alignment of the impulse response from the reverberation using only the beam formed data and avoids the need to access element data as is required for the DPCA. The capability to measure the impulse of the buried mine from a range of fifty meters and to measure the ping to ping correlation of the reverberation, for use in motion compensation, has been demonstrated. The program was terminated at this stage and the data has not been analyzed to form an image of the buried mine.

VII. DEVELOPMENT OF AN OPERATIONAL SONAR

While the tomographic imaging techniques have been demonstrated to provide images of the mines on the sea floor, they require a prior knowledge of where the mine has been detected to circumnavigate the target. An operational sonar must be able to also identify which patch of the sea floor should be imaged. To do this the sonar installed on the vessel also had a detection mode in which it operated as a side scan sonar. As the beam width of the sonar was wide compared to the range resolution, the mode of operation was modified to offset this limitation This was done by alternatively transmitting beams 10 degrees forward and 10 degrees aft of broadside. The displays were displaced fore and aft along the track and overlayed to give the display of fig. 25. In this display the two segments of the parabola, traced by the range variation along the track by the fore and aft beams, intersect to form a cross. This allows a cursor to be accurately positioned on the sonar display to determine the position of the target.

This was automatically processed by the navigation system to plot a circular track on the chart plotter which was used to circumnavigate the target to image the mines. This system was fully implemented on the Littoral Surveyor to provide an operational vessel for detecting and imaging buried and proud mines.

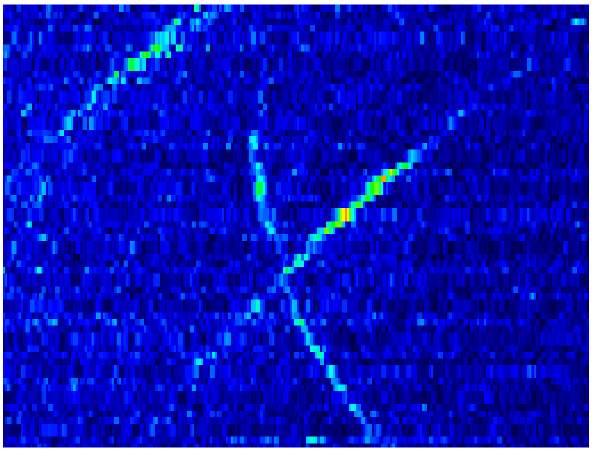

Fig. 26 The display from the detection sonar used to localize the targets.

ACKNOWLEDGMENT

The author gratefully acknowledges the contribution to the measurement of the data used in this paper by the Maritime Operations Division of DSTO, John Shaw, Neil Tavener, Mark Savage, Chris Halliday, Ross Susic, Jane Cleary and Tony White. Also the author acknowledges the contribution through ongoing discussions throughout the program with Brian Ferguson.

REFERENCES

[1] R.A. Altes and D.P. Skinner, "Doppler velocity resolution with a linear-period-modulate pulse," J. Acoust. Soc. Am. ,61 1019-1030, (1977).

[2] D.V. Sarwate and M.B. Pursely, "Crosscorrelation properties of pseusorandom and related sequences," Proc. IEEE, 68, 593-619. (1980).

[3] E.M.Kernaugh and.L. Moffet, "Transient and Impulse Response Approximations," Proc. IEEE, 53, 893-901, (1965).

[4] S. Qian and D. Chen, "Decomposition of the Wigner-Ville Distribution and Time-Frequency Distribution Series," IEEE Trans Sig. Proc., 42 ,2836-2842, (1984).